Supporting Online Material for

Label-Free, Single-Molecule Detection with Optical Microcavities

Andrea M. Armani, Rajan P. Kulkarni,
Scott E. Fraser, Richard C. Flagan, Kerry J. Vahala*

*To whom correspondence should be addressed. E-mail: vahala@caltech.edu

Published 5 July 2007 on *Science* Express
DOI: 10.1126/science.1145002

This PDF file includes:

Supplementary Online Material for
"Label-Free, Single-Molecule Detection with Optical Microcavities"

Detection Technique

Ultra-high-Q whispering gallery mode resonators are distinct from other resonant cavities, because of the very long photon lifetimes which can be achieved.(*1, 2*) In biodetection, these lifetimes give rise to improved sensitivity as described in (*3-8*). In the current report, they provide a double benefit through the thermo-optic detection mechanism which is responsible for the observed single-molecule detection sensitivity. Like other detection techniques, such as Surface Plasmon Resonance (SPR)(*9, 10*) or total internal reflection fluorescence microscopy (TIRF),(*11, 12*) the interaction which leads to detection occurs at the surface of the resonant cavity. As molecules bind to the surface of the microresonator, they interact directly with the evanescent tail of the whispering gallery mode (Fig. 1B).

Because it is the interaction of the molecule with the optical field which gives rise to detection events, the location of the molecule within the whispering gallery mode is important. As can be seen in Fig. 1B, the intensity profile of the evanescent tail is non-uniform over the surface of the toroid. Therefore, a molecule which binds at the highest intensity region of the whispering gallery will produce a signal significantly larger than one which binds at the lower intensity region. The interaction with this intensity profile produces a distribution in signals which can be easily seen in the histogram shown in Fig. 3C,D in the main text.

To detect this interaction, a single-mode, tunable external cavity laser centered at 681.5nm was coupled to a single-mode tapered optical fiber waveguide. Tapered optical fibers are very low-loss/high-efficiency waveguides used for probing ultra-high-Q modes in microcavities.(*13, 14*) They function both in air and in water and from the visible through the near-IR.(*1*) They were fabricated by heating F-SV optical fiber using an oxyhydric torch while stretching the fiber to an average waist diameter of 500nm.(*13*)

To create the testing chamber, the UHQ microtoroids were placed on a high-resolution translation stage and were monitored by two cameras (top and side view) simultaneously. With the taper waveguide in close proximity to the microtoroid, pure water was added and a cover slip was placed on top (Fig. S1), forming a water-filled microaquarium.(*1*) The gap between the tapered optical fiber waveguide determines the amount of power coupled into the microcavity and therefore could be determined using two techniques: by monitoring the gap using the top view camera (Fig. S2A, B) and by monitoring the input power into the microcavity.(*15*) Tapered optical fibers have previously demonstrated critical coupling (the condition when 100% of the power is coupled and dissipated into the resonant cavity) using both microtoroid and microsphere resonators.(*15, 16*) Therefore, these highly controllable waveguides are ideal for this application where the sensitivity of detection is directly proportional to input power. Solutions were injected into the aquarium and removed from the aquarium using a series of syringes at one end.

Both the intrinsic Q and resonant wavelength were determined by monitoring the power transmission spectra. The intrinsic Q factor was determined by scanning the wavelength of the single-mode laser and measuring both the resonant power transmission and the loaded linewidth (full-width-half-maximum) in the under-coupled regime. The intrinsic modal linewidth (and hence intrinsic Q) is then computed using a resonator-waveguide coupling model. (*13, 16*) The

position of the resonant frequency was determined by scanning the laser over a 0.03nm range and recording the resonance position from an oscilloscope.

The theoretical values in Fig. 4 in the main text were calculated at $Q=1x10^8$ and $Q=2x10^8$. However, achieving these precise Q factors experimentally is extremely difficult. The experimental data was taken on a series of resonators; the variation in the Q factor was approximately 25%.

This fact becomes significant in comparing the maximum shift in Fig. 3C and 3D. As noted in the figure legend, the Q value used in the pure IL-2 experiment was higher than the one used in the experiment in serum. This is not indicative of Q spoiling due to serum, but simply an artifact of the difference between the toroids used in the individual experiments.

Biological materials

The antibody-antigen pair that was chosen for this initial demonstration was the Interleukin-2 (IL-2) antigen and its corresponding polyclonal antibody which were obtained from Invitrogen. IL-2 is a cytokine released in response to immune system activation to extrinsic and intrinsic stimuli.(*17, 18*) The general antibody-antigen sensitization procedure is shown in Fig. S3A: 1) Protein G was bound to the surface of the toroid, 2) polyclonal IL-2 antibody was bound to the toroid surface via the affinity of Protein G for the Fc region of IgG,(*19*) and 3) IL-2 solution was injected into the bath surrounding the toroid. To perform the sensitization, first the microtoroid was immersed in water and an ultra-high-Q resonance coupled-to using a tapered optical fiber waveguide. Then the first solution (0.1μM Protein G) was added. After the Protein G formed a monolayer on the surface of the microtoroid (which triggered a red-shift in the resonant wavelength), the solution around the microtoroids was cleansed and refilled with fresh water. Then the second solution (0.1μM IL-2 antibody) was added. After the antibody formed a monolayer on the surface of the microtoroid (which triggered a second red-shift in the resonant wavelength), the solution around the microtoroids was cleansed and refilled with fresh water. Finally, the surface of the microtoroid was sensitized for IL-2 detection. A series of different IL-2 concentrations were used. Each solution was injected using a unique syringe, and the volume around the microtoroids was cleansed in between injections.

To perform single molecule measurements, the $3x10^{-16}$ M (300aM) solutions were used. At this concentration level, a low frequency of molecular binding events on the whispering gallery is expected. As each solution was added, the resonance position was recorded using an automated data acquisition system until the 1mL syringe was empty. The solution around the toroid was then cleansed by removing the ambient solution and replacing it with fresh water. Control tests were performed using either pure water or at dilution limits so low so as to make it unlikely for binding events to occur reliably. In these control tests either no shift (pure water) or infrequent shifts (extremely low dilution) were observed.

Additional proteins which were used in this study included: streptavidin, two distinct IL-2 antibodies, Cy5-labeled antibody, Protein G and QSY-21. (*20, 21*) Unique surface attachment protocols were developed for each of these proteins.

The streptavidin was specifically bound to the resonator using a biotin attachment (Fig. S3B). (*22*) In this protocol, 0.1 μM Biotin was attached to the surface of the microtoroid using physio-adsorption. After the Biotin formed a monolayer on the surface of the microtoroid (which

triggered a red-shift in the resonant wavelength), the solution around the microtoroids was cleansed to remove any free/unbound Biotin and refilled with fresh water. Then the streptavidin solution (300aM for the single molecule experiments) was added.

The polyclonal IL-2 antibodies and the Cy5-labeled antibody were attached to the toroid by first adsorbing Protein G onto the toroid, then binding the antibody to the Protein G. The microtoroid was exposed to a 0.1μM solution of Protein G which bound via physio-adsorption to the surface. The solution around the toroid was cleansed with fresh water to remove any free/unbound Protein G. The antibody or fluorescently labeled antibody was then injected into the volume. 300aM solutions were used for the single molecule experiments.

The QSY-21 was attached to the surface of the microtoroids using physio-adsorption. For the single molecule experiments, a 300aM solution was used.

To demonstrate detection in a more complex environment, we chose detection of Interleukin-2 (IL-2) in fetal bovine serum (FBS). An overview of the experimental outline is contained in Fig S4.While the Protein G surface functionalization is not ideal for detecting in serum because Protein G binds to other components in serum, the toroid can overcome this limitation because of the detection mechanism. Unlike conventional techniques, such as fluorescence which detects a single signal, the toroid is continuously detecting the resonant wavelength and is continuously providing information about its environment. Therefore, after the toroid is exposed to the pure serum which binds to any exposed Protein G, the zero point is re-set. The detection technique was identical to that outlined previously. The fetal bovine serum was diluted 10-fold to reduce its viscosity. Additional solutions using 10-fold diluted fetal bovine serum (FBS) doped with [300, 600, 900]aM of IL-2 were also prepared. The toroid was exposed to the pure serum twice: once to reset the zero position, and a second time for comparison with the solutions contained IL-2. This data is shown in Figs. 3B and 3D in the main text.

Thermal Stabilization

Owing to the ultra-high-quality factors of toroidal microcavities, these devices tend to be sensitive to thermal effects.(*23, 24*) It has previously been shown that these effects can be used to thermally lock a microcavity to a laser source(*25*) or thermo-optically tune the resonant wavelength of the microcavity.(*26*) When performing ultra-sensitive biological and chemical detection experiments with microcavities, the detection event is determined by monitoring the resonant wavelength and lineshape.(*27, 28*) Therefore, it is important to optimize the stability of the resonant wavelength under ambient conditions.

When detection experiments are performed, the entire microcavity is immersed in an aqueous environment (Fig. S1).(*1*) This experimental set-up is very different to previous studies in air for several reasons. Because both silica and air have negative thermo-optic coefficients (dn/dT), these microcavities generally experience wavelength red-shifts in air when optical power is applied.(*23*) However, the thermo-optic coefficient of water is positive.(*29*) It is possible to use this effect to neutralize the overall thermal shift produced by the circulating power heating of both the silica and the surrounding water. The condition of neutrality occurs for a specific spatial overlap of the whispering gallery mode with the water and can be computed using a COMSOL Multiphysics 3.2 finite element code with the Chemical Engineering Module.

This overlap, in turn, corresponds to a specific whispering-gallery diameter. If the system moves away from this neutrality condition (i.e., toroid diameter is too large or too small), then the resonant wavelength either red-shifts (diameter is too large and silica component of index shift is dominant) or blueshifts (diameter is too small and water component of index shift is dominant). While this effect is present in all microcavity devices, it would be most apparent in an ultra-high-Q cavity, due to the high circulating intensities present, which would lead to higher temperature gradients.

To experimentally verify this effect and to demonstrate the neutrality condition, a series of ultra-high-Q microtoroids with a range of major and minor diameters (Fig. S5) were fabricated.(*2*) The microtoroid resonators are an ideal platform to study this effect as the major and minor diameter can be very accurately controlled during the photolithographic fabrication process. This control allows for precise "dialing in" of the modal overlap with the aqueous environment and demonstration of the neutrality condition. Plots showing the fraction of circulating power within the toroid versus minor diameter for a series of major diameters are provided in Fig. S6.

Measurements of the resonator wavelength and resonance shift were performed as detailed previously. For large diameters, the resonant wavelength is observed to red-shift as the coupled optical power is increased (Fig. S7). However, as the modal overlap with the water increases (the major diameter decreases), the resonant wavelength begins to blue shift when the power is increased. A close-to-neutral-shift toroid is also observed in Fig S7 (major diameter of 80 microns). The theoretical prediction based on the COMSOL model is shown as dashed lines in Fig. S7. There is excellent agreement between the experimental data and the finite element modeling across all major and minor microtoroid diameters and input powers.

Finally, it is important to distinguish this neutrality condition and its underlying physics from the opto-thermal effect used to detect single molecule shifts. In particular, the neutrality condition creates a balance in contributions to resonator optical path length changes produced by heating of the water and the silica. This balance does not, however, negate the thermal-induced shift created by local heating of a bound molecule.

Statistical Analysis

Data showing the resonance position as a function of time is presented in Fig. S8 for three concentrations [100, 300, 600]aM of IL-2. This data is reproduced from Figure 3A in the main text. As expected, the slope of this line changes with concentration because it is proportional to the average binding rate. At the data acquisition rate used in these experiments, individual binding events can be resolved.

If the probability of observing a single molecule event is time independent, it can be approximated as a Poissonian process. In Fig. S9, the number of "no binding events," N, is measured using raw data such as in Fig. S8. For a Poissonian process the relation $\ln(N)=\ln(N_o) - t/\tau$ is expected to hold for all concentrations (C) and injection rates where single molecule events are resolvable. N_o in this expression is the total number of events sampled and $1/\tau$ is the average rate. This relation was verified for a series of concentrations (Fig. S9A), and the linear relation between τ and inverse concentration (C^{-1}) is observable in Fig. S9B.

At higher concentrations, the probability of seeing multiple events in a single time interval increases, since the data acquisition rate is constant. Figure S10 is a histogram showing binding

count versus shift at a higher concentration. The data in Fig. 3C of the main text shows a maximum shift that is independent of concentration, which, as noted in the main text, results from single molecule binding at the equatorial plane. In Fig. S10 this cutoff is replaced by a "tail" in the histogram, indicating the presence of events in which multiple binding has occurred within the data collection sampling time.

Detection Mechanism

As noted in the text, the majority of biological molecules have minimal impact on the cavity Q factor, and therefore the Q remains relatively constant throughout a single molecule experiment. However, if a highly absorbing molecule is used, such as a fluorescent dye, then the Q will decrease. This decrease can be directly incorporated into the thermo-optic detection mechanism by adding the molecule in as an additional loss mechanism where the molecule contributes to the contamination loss:

$$Q_{tot}^{-1} = Q_{mat}^{-1} + Q_{ss}^{-1} + Q_{rad}^{-1} + Q_{coup}^{-1} + Q_{cont}^{-1} \tag{S1}$$

where Q_{mat} is material loss, Q_{ss} is surface scattering loss, Q_{rad} is whispering gallery loss, Q_{coup} is coupling loss, and Q_{cont} is contamination loss. (*30*) When a highly absorbing molecule is used, the decrease in the quality factor from the initial Q (Q_i) to the Q after binding (Q_f) can be predicted according to the following formula:

$$Q_f = \frac{Q_m Q_i}{Q_m + Q_i} \tag{S2}$$

where Q_m is the quality factor of the ideal resonator with no other loss mechanism than that induced by a single molecule bound to the whispering gallery. Molecules that have very high cross sections induce low Q_m values.

Concerning the photo-thermal-induced wavelength shift, it is actually Q_f that is important in determining this shift as the steady-state circulating intensity is determined by this value. Replacing Q in equation (1) of the main article with the expression above, the new expression for $\delta\lambda$ upon binding of a single molecule of cross section σ is:

$$\left[\frac{\delta\lambda}{\lambda}\right]_{SM} = \frac{\sigma\lambda\, {}^{dn}\!/_{dT}}{8\pi^2 n^2 \kappa V} \frac{Q_m Q_i}{Q_m + Q_i} P \int \frac{|u(\vec{r})|^2}{|\vec{r}| + \varepsilon} d\vec{r} \tag{S5}$$

It should be stressed that the thermo-optic mechanism is not limited to ultra-high-Q silica resonant cavities and can be generalized to other lower-Q resonant cavities, provided that power levels are substantially boosted to overcome the reduced Q. Thus, the opto-thermal detection mechanism is universal, as it can be applied across a wide range of molecules and optical microcavities.(*31-37*)

In the majority of regimes (single molecule antibody and antigen experiments), this expression will simplify to (1) because Q_f and Q_i are nearly identical. However in the present work there are some experiments that require this more complex formula because the absorption cross sections are sufficiently large and change the optical quality factor upon binding. Cy5 and QSY-21 are examples. The saturation observable in the otherwise linear behavior within Fig. 4 of the main text is one example of this effect. However, it is important to note that both of these molecules are synthetic and would not be present in a natural environment, such as serum or lysate.

Single Molecule Photo-bleaching

In addition to the experiments detailed in the main text, a single molecule photo-bleaching experiment was designed using a Cy5 labeled antibody.(*38*) While this fluorescent probe's absorption maximum is 645nm, the tail of the absorption overlaps with the 680nm resonance. Therefore, it is possible to photobleach this dye using a 680nm excitation source. Detecting a fluorescent species with an ultra-high-Q planar microcavity has been proposed previously but had never been experimentally realized until now.(*3*)

The Cy5 labeled antibody was immobilized on the surface of the microtoroids as detailed above and shown in Fig. S3. The resonant wavelength location in H_2O was taken for 5 minutes after being sensitized with Protein G. Then the Cy5 labeled antibody was injected into the bath surrounding the microtoroid. It is important to note that the microtoroid only interacts with molecules bound to the surface when it is on-resonance. Therefore, this experiment is analogous to a pulsed-laser excitation of fluorescent molecules, not a continuous wave excitation experiment, as is more commonly performed.(*38*) It has been shown that the fluorescent lifetime of Cy5 is extended when it is excited using a pulsed diode laser in contrast to a continuous wave laser.(*20*) Additionally, in this experiment, Cy5 is being excited at 680nm. At this wavelength, the absorption of the dye is decreased by over 85% as compared to its maximum absorption wavelength which is located around 645nm.(*39*)

Both the resonant wavelength shift and the optical quality factor were monitored in the experiment. A low concentration solution was injected until a response was observed. This concentration was selected based on prior results to ensure that only a few molecules would bind to the whispering gallery. Initially, a step shift in wavelength and Q factor were observed as seen in the data of Fig. S11. Cy5 has a large enough absorption cross section to cause a substantial modification to the optical quality factor even in cases where only a single molecule binds. As shown in Fig. S11 (a and b), over time a sequential bleaching is observed, suggesting that two Cy5 molecules are observed. Estimates of Q shifts for binding of two Cy-5 molecules are in the range of the observed initial Q shift, furthering suggesting that the bleaching data are representative of individual molecules. It should be noted that the resonant shift does not return to zero or the initial position. The existence of this residual shift is further evidence that the Cy5 was photo-bleached and did not simply detach from the surface of the cavity.

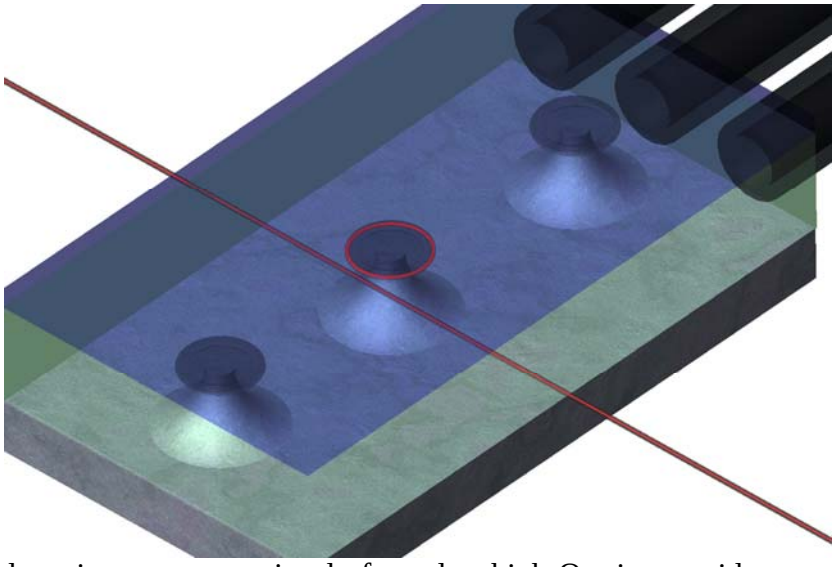

Figure S1: The detection set-up consisted of an ultra-high-Q microtoroid resonator coupled to a low-loss tapered optical fiber. In the rendering, the microtoroid resonator is shown operating on-resonance, when light is coupled into the whispering gallery mode of the microcavity. Solutions were added into the micro-aquarium surrounding the resonator via a series of syringes at one end.

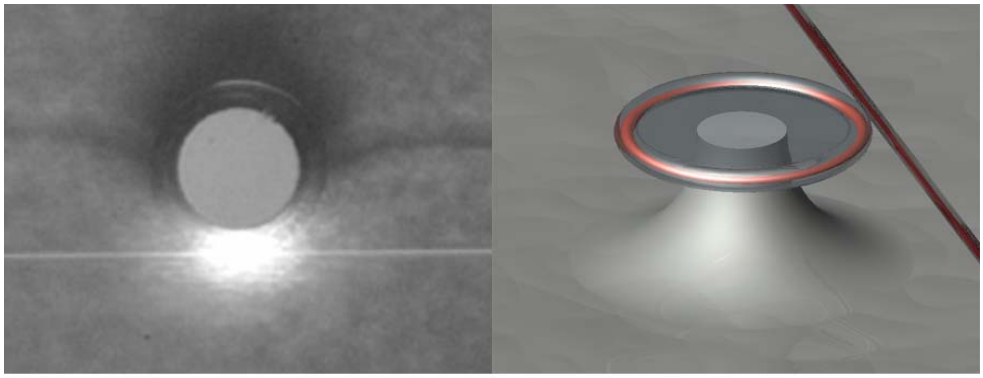

Figure S2: The microtoroid optical resonator coupled to a tapered optical fiber. (A) An optical micrograph of the microtoroid immersed in water coupled to a tapered optical fiber. (B) A rendering showing the microtoroid resonator coupled to a tapered optical fiber and highlighting the location of the whispering gallery mode in the microtoroid resonator.

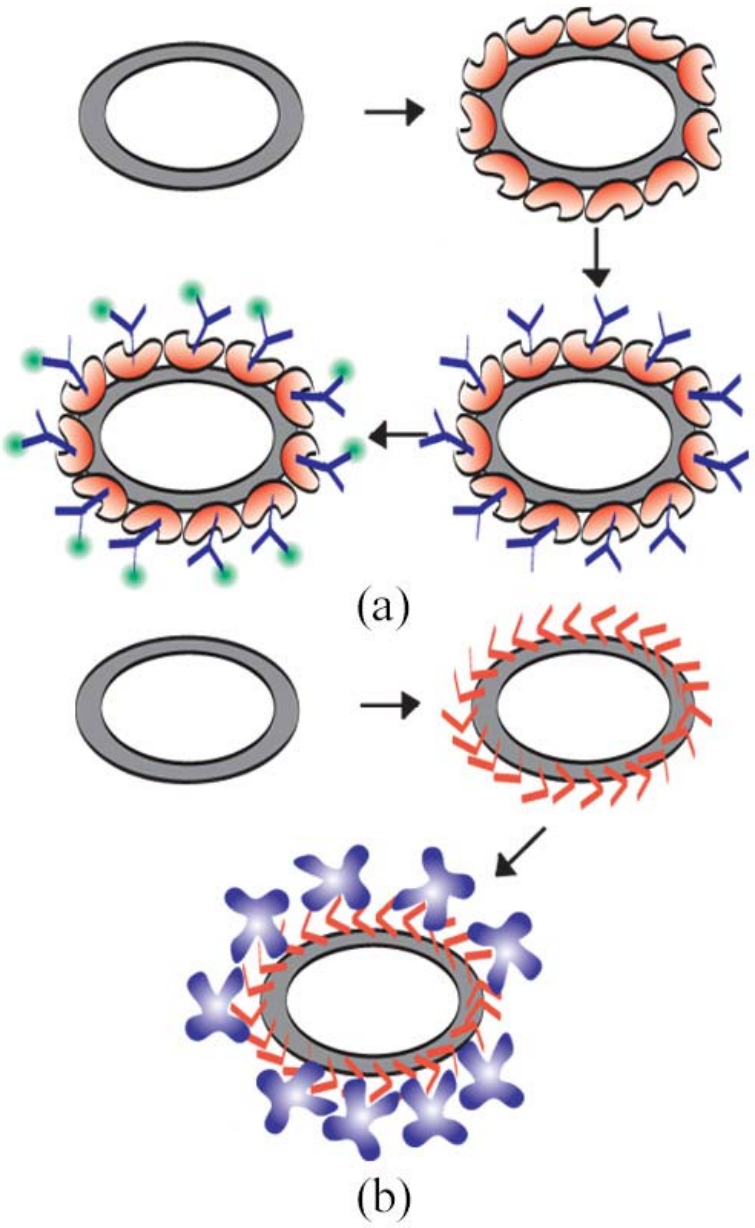

Figure S3: Two different sensitization techniques were employed: (A) antibody-antigen and (B) biotin-streptavidin. (A) The sensitization process for the antibody-antigen pairs has four steps: i) placing toroidal resonator in water, ii) coating the silica surface of the microtoroid with Protein G (red), iii) attaching polyclonal anti-IL-2 (blue) to the Protein G, and iv) specifically binding human IL-2 (green) to the polyclonal antibody. Protein G was a necessary intermediate because it attached the antibody to the surface of the resonator with the antigen binding sites facing the aqueous environment. The polyclonal antibody enabled targeted, label-free detection of IL-2. (B) The process for the biotin-streptavidin detection has three steps: i) placing toroidal resonator in water, ii) coating the silica surface of the microtoroid with Biotin (red), and iii) specifically binding streptavidin (blue) to the biotin.

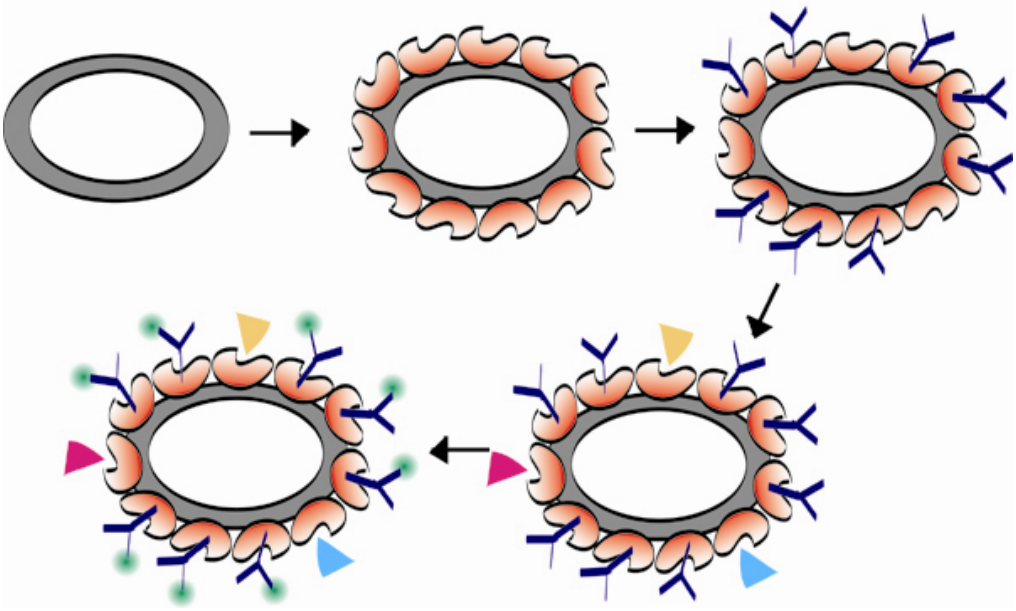

Figure S4: Surface sensitization and experiment outline: i) immerse toroid in water, ii) expose to Protein G (red), iii) Expose to anti-IL2 (blue), iv) expose to pure serum (various components in serum will bind to protein G, indicated by triangles), v) expose to series of serum solutions containing known amounts of IL-2 (green).

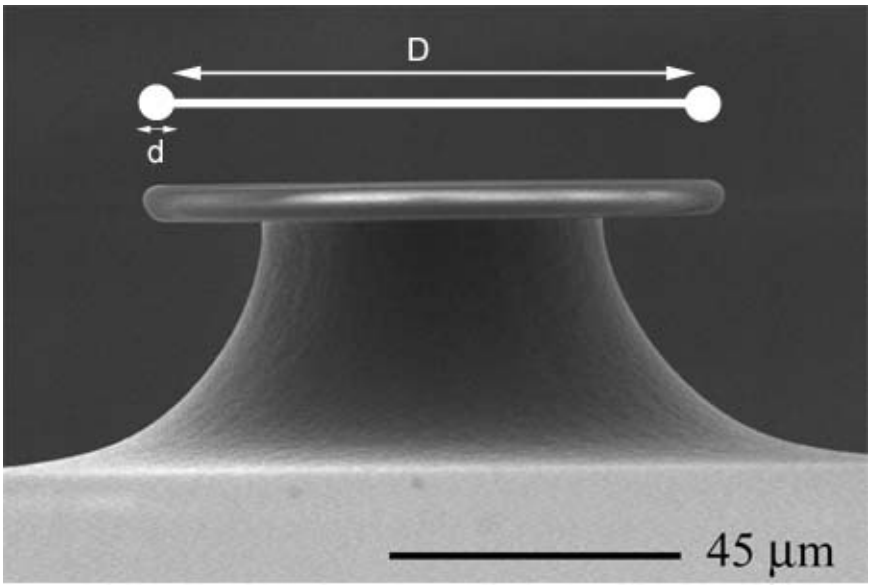

Figure S5: Scanning electron micrograph which highlights the geometry of the microtoroid and identifies the major (D) and minor (d) diameters which were varied to achieve the neutrality condition.

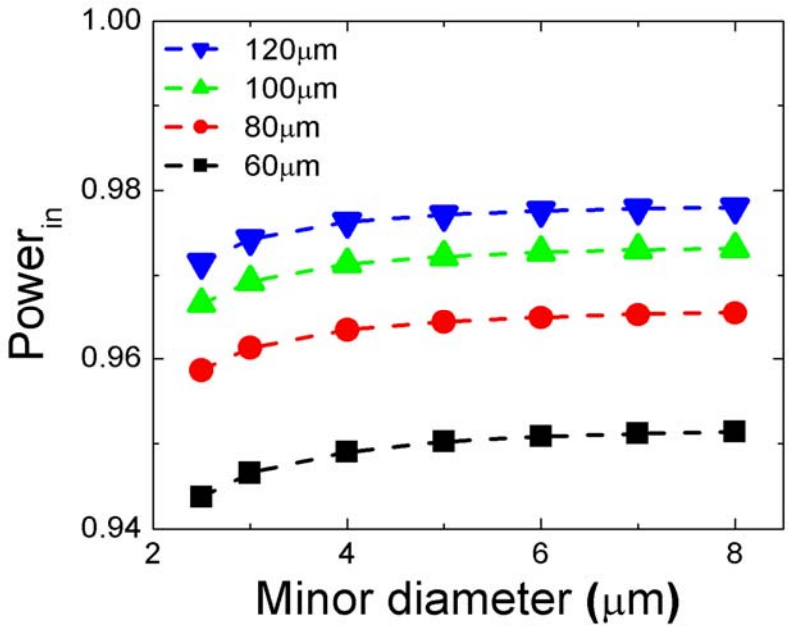

Figure S6: FEMLAB modeling of the optical mode in the toroid at a series of major and minor diameters. Modeling was performed at discrete microtoroid major/minor diameters. Lines were added to show the overall trend based on the modeling. Plot shows the power overlap with the dielectric microcavity versus minor diameter and with major diameter as a parameter.

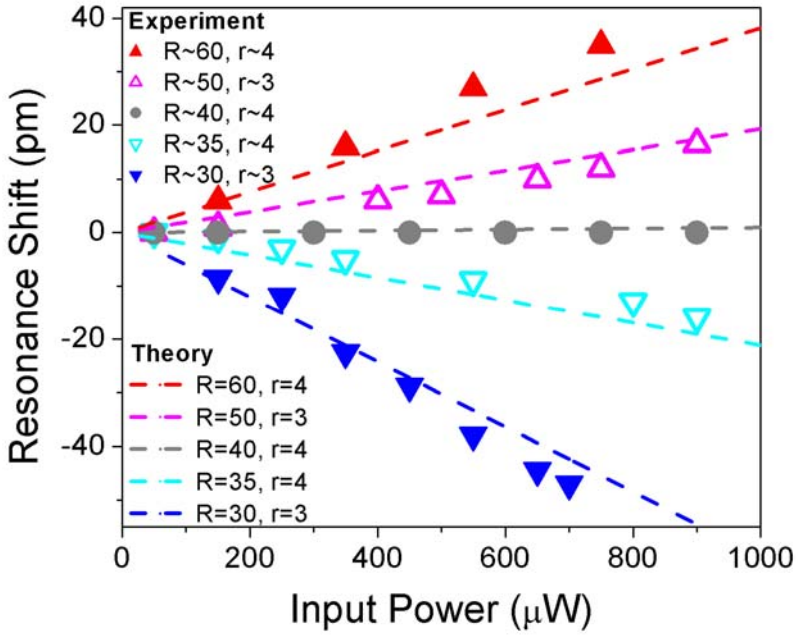

Figure S7: Measured tuning of the whispering gallery mode versus coupled optical power. Each data set corresponds to the major and minor radii indicated (in microns). Larger radii experience a red shift while smaller radii experience a blue shift with increasing coupled power. At a diameter of about 80 microns, the neutrality condition is observed. The dashed lines are the predictions based on the model.

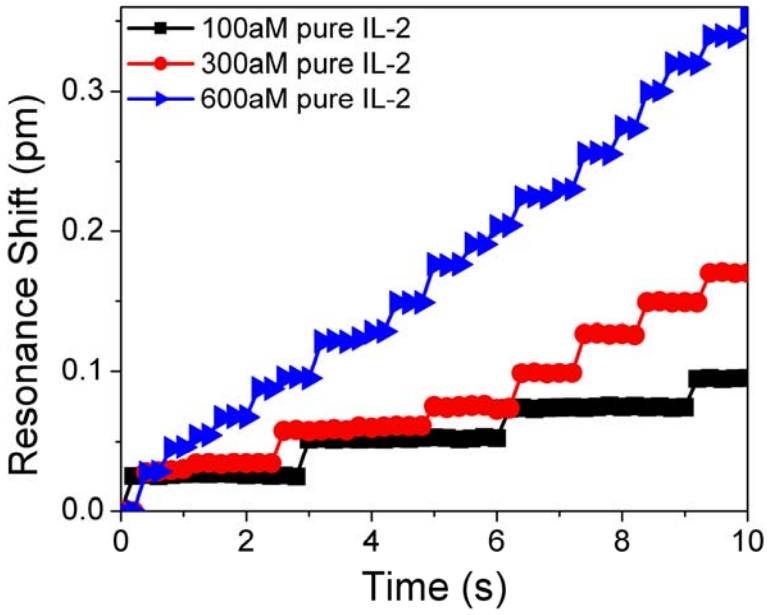

Figure S8: The position of the resonance wavelength as a function of time at three different IL-2 concentrations. As molecules bind to the surface, the resonant wavelength position jumps, creating the steps seen. When the concentration is increased, the general slope of the trace increased because the number of binding events increased. It is important to note that discreet binding events are resolved at this data acquisition rate. Reproduced from Figure 3A in the main text.

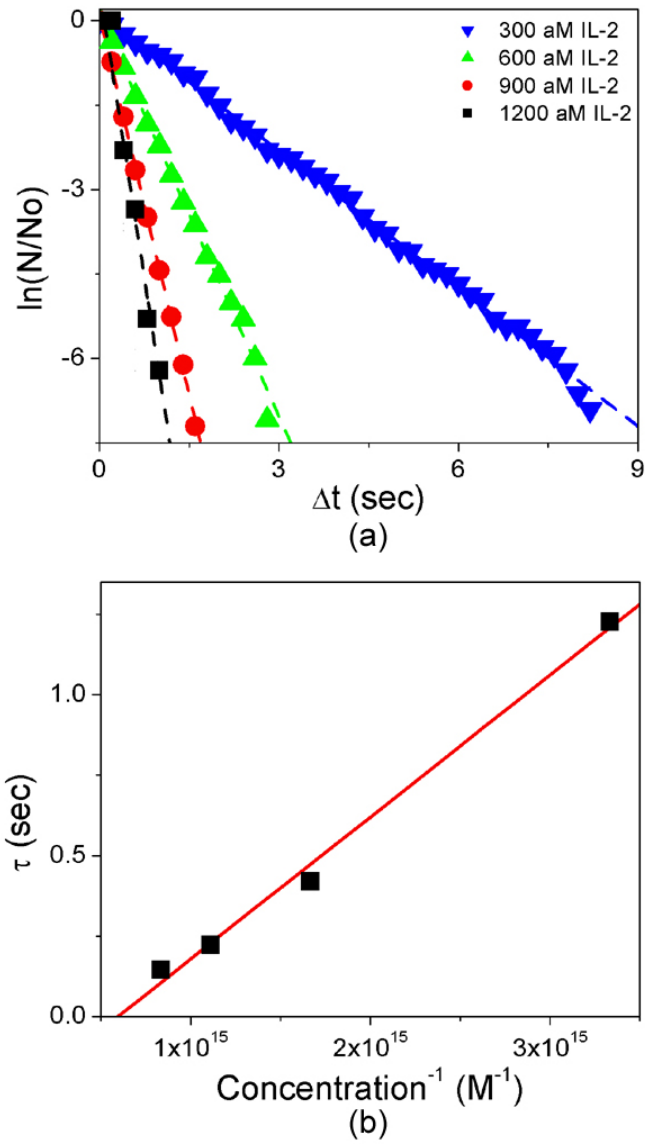

Figure S9: The number of non-events vs. time for a series of IL-2 concentrations. (A) As the concentration increases, the time between unique events decreases. (B) A plot of τ, as inferred from the slopes in part A, versus inverse-concentration verifies the expected linear dependence.

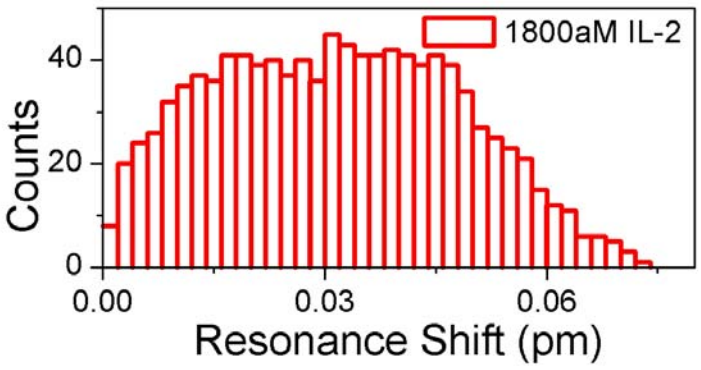

Figure S10: A histogram of an 1800aM IL-2 solution showing the breakdown in the behavior that was seen in the lower concentration data in Fig. 3C and 3D of the main text. This data was part of a series of measurements used to determine the optimum balance between data acquisition rate and IL-2 concentration. As the concentration is increased beyond a threshold, multiple binding events occur in a single measurement sampling time period. The bin size in this plot is 0.002pm.

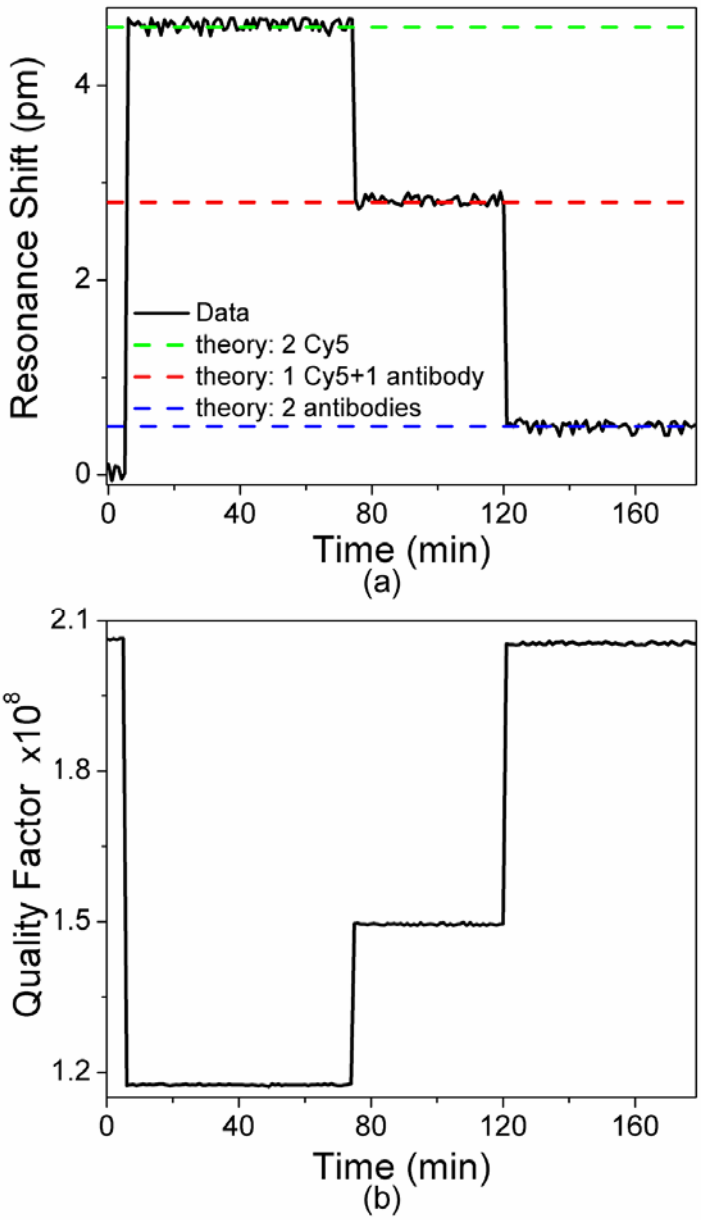

Figure S11: Cy5 labeled antibody photo bleaching data. (A) Photobleaching of two Cy5 fluorescent molecules. Binding of two Cy5 fluorescent labeled antibodies produces, at first, a red shift in the resonant wavelength, followed by two, sequential, blue-shifts versus time as the two Cy5 molecules are photobleached. (B) Coincident with the observed wavelength-shifts is a decrease and then sequential recovery of the microtoroid's quality factor.

References

1. A. M. Armani, D. K. Armani, B. Min, K. J. Vahala, S. M. Spillane, *Applied Physics Letters* **87**, 151118 (Oct 10, 2005).
2. D. K. Armani, T. J. Kippenberg, S. M. Spillane, K. J. Vahala, *Nature* **421**, 925 (Feb 27, 2003).
3. S. Blair, Y. Chen, *Applied Optics* **40**, 570 (Feb 1, 2001).
4. R. W. Boyd, J. E. Heebner, *Applied Optics* **40**, 5742 (Nov 1, 2001).
5. S. Arnold, M. Khoshsima, I. Teraoka, S. Holler, F. Vollmer, *Optics Letters* **28**, 272 (Feb 15, 2003).
6. C. Y. Chao, L. J. Guo, *Journal of Lightwave Technology* **24**, 1395 (Mar, 2006).
7. E. Krioukov, D. J. W. Klunder, A. Driessen, J. Dreve, C. Otto, *Optics Letters* **27**, 512 (2002).
8. A. Ksendzov, Y. Lin, *Optics Letters* **30**, 3344 (2005).
9. K. Nakatani, S. Sando, I. Saito, *Nature Biotechnology* **19**, 51 (Jan, 2001).
10. F. Sundberg, R. Karlsson, *Immunology* **120**, 46 (Mar, 2007).
11. A. Hoshino *et al.*, *Microbiology and Immunology* **49**, 461 (2005).
12. T. Funatsu, Y. Harada, M. Tokunaga, K. Saito, T. Yanagida, *Nature* **374**, 555 (Apr 6, 1995).
13. S. M. Spillane, T. J. Kippenberg, O. J. Painter, K. J. Vahala, *Physical Review Letters* **91** (Jul 25, 2003).
14. M. Cai, K. Vahala, *Optics Letters* **26**, 884 (Jun 15, 2001).
15. T. J. Kippenberg, S. M. Spillane, D. K. Armani, K. J. Vahala, *Applied Physics Letters* **83**, 797 (Jul 28, 2003).
16. M. Cai, O. Painter, K. J. Vahala, *Physical Review Letters* **85**, 74 (Jul 3, 2000).
17. C. S. Henney, K. Kuribayashi, D. E. Kern, S. Gillis, *Nature* **291**, 335 (1981).
18. M. C. Mingari *et al.*, *Nature* **312**, 641 (1984).
19. B. M. Kihlberg, U. Sjobring, W. Kastern, L. Bjorck, *Journal of Biological Chemistry* **267**, 25583 (Dec 15, 1992).
20. C. Eggeling *et al.*, *Journal of Physical Chemistry A* **110**, 2979 (Mar 9, 2006).
21. I. L. Medintz, E. R. Goldman, M. E. Lassman, J. M. Mauro, *Bioconjugate Chemistry* **14**, 909 (Sep-Oct, 2003).
22. L. A. Klumb, V. Chu, P. S. Stayton, *Biochemistry* **37**, 7657 (May 26, 1998).
23. H. Rokhsari, S. M. Spillane, K. J. Vahala, *Applied Physics Letters* **85**, 3029 (Oct 11, 2004).
24. A. E. Fomin, M. L. Gorodetsky, I. S. Grudinin, V. S. Ilchenko, *Journal of the Optical Society of America B-Optical Physics* **22**, 459 (Feb, 2005).
25. T. Carmon, L. Yang, K. J. Vahala, *Optics Express* **12**, 4742 (Oct 4, 2004).
26. D. Armani, B. Min, A. Martin, K. J. Vahala, *Applied Physics Letters* **85**, 5439 (Nov 29, 2004).
27. A. M. Armani, K. J. Vahala, *Optics Letters* **31**, 1896 (Jun 15, 2006).
28. F. Vollmer, S. Arnold, D. Braun, I. Teraoka, A. Libchaber, *Biophysical Journal* **85**, 1974 (Sep, 2003).
29. J. H. Burnett, S. G. Kaplan, *Journal of Microlithography Microfabrication and Microsystems* **3**, 68 (Jan, 2004).
30. D. W. Vernooy, V. S. Ilchenko, H. Mabuchi, E. W. Streed, H. J. Kimble, *Optics Letters* **23**, 247 (Feb 15, 1998).
31. A. M. Armani, A. Srinivasan, K. J. Vahala, *Nano Letters* **7** (2007).
32. M. Borselli, T. J. Johnson, O. Painter, *Optics Express* **13**, 1515 (Mar 7, 2005).
33. P. Rabiei, W. H. Steier, *Ieee Photonics Technology Letters* **15**, 1255 (Sep, 2003).
34. K. J. Vahala, Ed., *Optical Microcavities* (World Scientific, 2004), pp.
35. P. E. Barclay, K. Srinivasan, O. Painter, B. Lev, H. Mabuchi, *Applied Physics Letters* **89** (Sep 25, 2006).
36. K. Srinivasan, M. Borselli, O. Painter, *Optics Express* **14**, 1094 (Feb 6, 2006).
37. M. C. M. Lee, M. C. Wu, *Ieee Photonics Technology Letters* **17**, 1034 (May, 2005).
38. E. Fureder-Kitzmuller, J. Hesse, A. Ebner, H. J. Gruber, G. J. Schutz, *Chemical Physics Letters* **404**, 13 (Mar 7, 2005).
39. G. L. Ferri, J. Isola, P. Berger, G. Giro, *Journal of Histochemistry & Cytochemistry* **48**, 437 (Mar, 2000).